NANO LETTERS

pubs.acs.org/NanoLett Letter

Database Construction of Two-Dimensional Charged Building Blocks for Functional-Oriented Material Design

Jun Deng, Jinbo Pan, Yan-Fang Zhang, and Shixuan Du*

Cite This: *Nano Lett.* 2023, 23, 4634−4641 Read Online

ACCESS | Metrics & More | Article Recommendations | Supporting Information

ABSTRACT: Databases for charge-neutral two-dimensional (2D) building blocks (BBs), i.e., 2D materials, have been built for years due to their applications in nanoelectronics. Though lots of solids are constructed from charged 2DBBs, a database for them is still missing. Here, we identify 1028 charged 2DBBs from Materials Project database using a topological-scaling algorithm. These BBs host versatile functionalities including superconductivity, magnetism, and topological properties. We construct layered materials by assembling these BBs considering valence state and lattice mismatch and predict 353 stable layered materials by high-throughput density functional theory calculations. These materials can not only inherit their functionalities but also show enhanced/emergent properties compared with their parent materials: CaAlSiF displays superconducting transition temperature higher than NaAlSi; Na_2CuIO_6 shows bipolar ferromagnetic semiconductivity and anomalous valley Hall effect that are absent in $KCuIO_6$; LaRhGeO possesses nontrivial band topology. This database expands the design space of functional materials for fundamental research and potential applications.

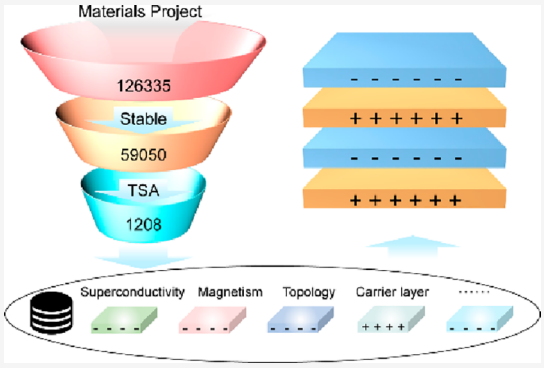

KEYWORDS: *charged building block database, density functional theory, functional-oriented materials design, superconductivity, ferromagnetic semiconductor, topological material*

Downloaded via INST OF PHYSICS on May 24, 2023 at 09:21:32 (UTC).
See https://pubs.acs.org/sharingguidelines for options on how to legitimately share published articles.

Layered materials are built from staggered stacking of two-dimensional (2D) units, which are of great interest for their diverse physical and chemical properties. In terms of the coupling between the 2D units, they can be categorized into two groups, i.e., van der Waals (vdW) layered structures and ionic layered structures.[1] In vdW layered materials, these 2D units are charge neutral and coupled by weak vdW interactions. In contrast, in ionic layered structures, they are charged with stronger interlayer bonding. The stacking of different functional vdW units turns out to be an effective way to modulate the interplay of charge and spin correlations with enhanced and emergent properties.[2−6] However, the design of functional materials based on these charged building blocks is relatively unexploited.

Constructing layered materials from these charged 2D units has been a research frontier for decades. New layered materials can be designed by rationally stacking charged units with commensurate lattice and charge neutrality.[7−11] For example, the well-known layered compound LaFeAsO can be considered as stacking charged $[La_2O_2]^{2+}$ and $[Fe_2As_2]^{2-}$ layers. Intriguingly, tailoring the charge state of $[La_2O_2]^{2+}$ layer makes $[Fe_2As_2]^{2-}$ in a hole or electron doped state, e.g., substituting La with Ce/Pr/Gd/Sr or O with F, which effectively suppresses the antiferromagnetic ordering and induces superconductivity.[12−16] It is deemed that in LaFeAsO, $[Fe_2As_2]^{2-}$ layer is responsible for superconductivity and $[La_2O_2]^{2+}$ provides carriers.[17] Similar cases occur in $[Bi_2O_2]$-based thermoelectric material,[18−20] $[Mn_2As_2]$-based magnetic materials,[21−24] and $[CuO_2]$-based[25] and $[Fe_2X_2]$-based (X = As, Se)[26] high-temperature superconductors, where the physical properties mainly attribute to the specific functional building blocks. Thus, in ionic layered structures, particular layers mostly determine the physical property of the crystal, i.e., functional building blocks, and the remaining ones are carrier providers (charge compensators). Carefully engineering functional building blocks and their charge compensators enables the possibility of functional-oriented material design (Figure 1a), which is a main goal in materials science,[27−29] while the search of functional building blocks and charge compensating layers is still by serendipity, which hinders the design of layered functional materials. Therefore, it is highly desirable to construct the database of charged layered building blocks for functional-oriented material design.

In this work, we use a topological scaling algorithm (TSA)[30] to identify the 2D charged building blocks from materials in Materials Project database and discovered 1208 2D charged

Received: April 1, 2023
Revised: May 1, 2023
Published: May 5, 2023

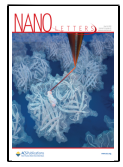

ACS Publications © 2023 American Chemical Society

https://doi.org/10.1021/acs.nanolett.3c01237
Nano Lett. 2023, 23, 4634−4641

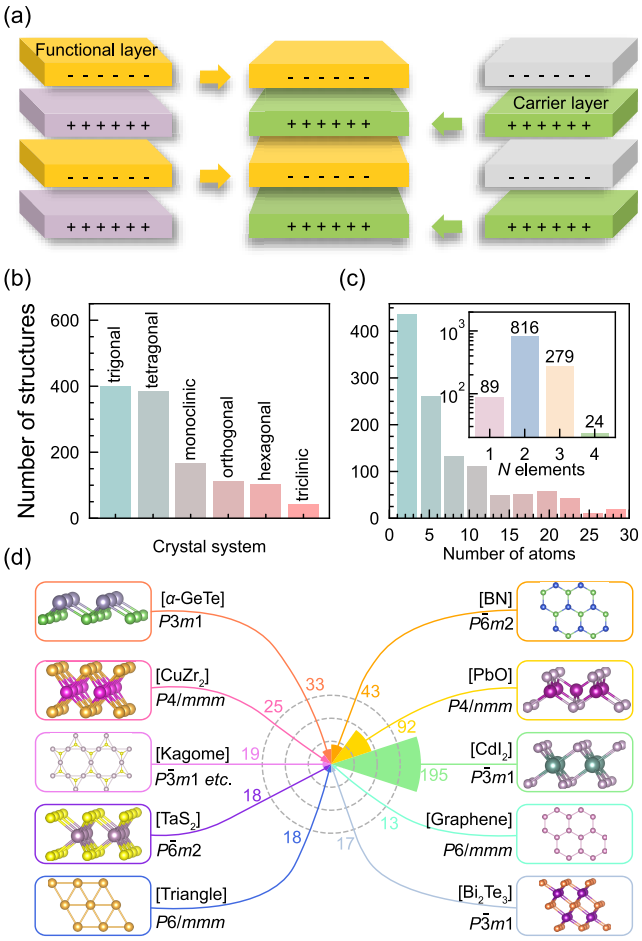

Figure 1. Statistics of 2D charged building blocks. (a) Schematic diagram of constructing functional materials from charged building blocks. The new functional material (middle) is assembled by stacking a functional layer and a carrier layer with charge- and lattice-matched building blocks. (b) Distribution of crystal system and (c) number of structures as a function of number of atoms in the unit cell for the screened 2D charged building blocks. Here, the structures with number of atoms larger than 30 are omitted. The inset shows the distribution of unique elements in the building blocks for them. (d) Some typical prototypes of 2D charged building blocks.

ones. These building blocks have fruitful structural prototypes, crystal systems, elemental distributions, and functionalities which are ideal for designing new functional materials. Next, utilizing the 2D tetragonal/hexagonal/trigonal units in the database, we build a workflow to construct layered materials. By high-throughput density functional theory (DFT) calculations, we identify 353 of them that are thermodynamically and lattice-dynamically stable. Finally, materials with superconductivity, bipolar ferromagnetic semiconductivity with valley polarization, and nontrivial band topology are found among these materials, which deserve further experimental verification.

CONSTRUCTION OF 2D CHARGED BUILDING BLOCKS DATABASE

We start with materials from Material Project (MP) database,[31] which contains 126 335 entries. To guarantee the high quality of our building block database, only those with ICSD collection codes or E_{hull} = 0 eV/atom are left for further consideration, where the E_{hull} is the energy above convex hull.[32,33] The building blocks hidden in alkaline metals (AM) and alkaline earth metals (AEM) intercalated structures are additionally considered by removing AM and AEM in these structures. We show this procedure is very important for these intercalated structures in finding charged building blocks in Figure S1. Then these 2D layers can be identified by the TSA.[30] Next, we consider the ones with the same nominal elemental ratio as their parent as van der Waals (vdW) networks, and the others are charged ones. Finally, we keep 2D charged layers as building blocks to construct the database and the rationalization of them is visually checked, which yields 1208 entries. The overall workflow for screening the charged building blocks is shown in Figure S2.

We identify the charge states for these building blocks. First, we determine the valence states of their parent compounds implemented with the pymatgen package.[34] It considers all the combinations of common elemental oxidation states and gives the charge-balanced result. Although it sometimes fails to resolve the valence state, e.g. setting zero valence state for all elements in the compound, most of them can be properly calculated with a right valence state. Next, the valence states of the building blocks are derived from their parent compounds. It should be noted that a building block can own multiple valence states, e.g., $[Fe_2As_2]^{\delta-}$ layer has different valence state, −1 in KFe_2As_2[35] and −2 in $BaFe_2As_2$[36] (both crystallize with $ThCr_2Si_2$ structural prototype).

Figure 1b−d shows the distribution of crystal systems, number of atoms/elements, and typical prototypes for these 2D charged building blocks. Our statistics show that trigonal and tetragonal crystal systems are the most common ones in Figure 1b. And around 73% of them have number of atoms less than 10 displayed in Figure 1c. Besides, most of them are binary and ternary ones. We note that some of the unary ones are alkaline and alkaline earth metals. We still keep them to enrich the database and use them to build intercalated structures in the procedures below. We also classify them into different prototypes. Some examples of prototypes are illustrated in Figure 1d. The most common structural prototype is $[CdI_2]$-type which contains 195 structures in this set. Although these prototypes are reported, most of them are not suggested as charged building blocks for material design before. And it is believed that the functionality of the building blocks can be inherited from their parent compounds. For example, [PbO]-type charged units often host superconductivity (such as [FeAs],[12] [FeP],[37] [FeSe][38]), which are ideal building blocks for designing superconductors; kagome building blocks manifest itself with flat band and Dirac point, which are potential candidates to explore correlated and topological electronic states, etc. The versatility of these building blocks will be beneficial to explore functional materials. A full list of these building blocks and their potential functionalities are provided in Supporting Information.

CONSTRUCTING LAYERED STRUCTURES AND HIGH-THROUGHPUT CALCULATIONS

Having established the charged building block database, we utilize them to systematically design new functional materials. Figure 2 shows our workflow for constructing new layered structures. To facilitate the procedures, only hexagonal, trigonal, and tetragonal building blocks with number of atoms less than 10 are considered for further processing, which yields 797 ones. We stack two building blocks with the same symmetry and lattice mismatch[8] (constrained in the

https://doi.org/10.1021/acs.nanolett.3c01237
Nano Lett. 2023, 23, 4634−4641

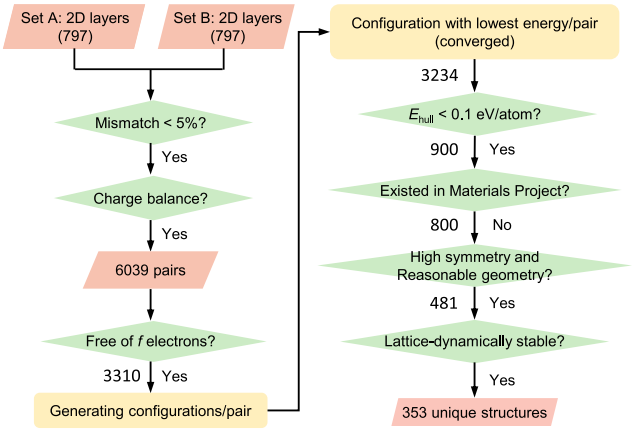

Figure 2. Workflow for construction of layered materials by stacking 2D charged building blocks. Here, we only consider 797 2D charged building blocks with tetragonal, trigonal, and hexagonal symmetry and number of atoms less than 10 as input to construct layered structures. The numbers on the left side of each procedure show the remaining ones after a specific procedure.

primitive cell); i.e., tetragonal building blocks stack on tetragonal ones, and hexagonal/trigonal ones stack on hexagonal/trigonal ones. Considering the intrinsic lattice variation of building blocks and the mismatch tolerance widely used in vdW heterostructures[39,40] and solid−solid interfaces,[41,42] here we use a 5% mismatch tolerance. Next, ensure that they are in a charge balanced state.[8] For building blocks with multiple valence states, combinations of them are made and those with a net zero charge state are considered as a reasonable pair, which generates 6039 ones. For each pair, we also considered different stacking orderings and rotational/mirror operations. The details can be found in Figures S3−S5. Here, we only consider cationic building blocks in the database with the match of charge and lattice for a specific anion. It is also worth trying other possible choices of cationic building blocks that are not in our database.

After building layered structures for each pair with different stacking configurations, we resort to density functional theory (DFT) calculations under the Perdew−Burke−Ernzerhof (PBE)[43] level to find the most stable one for each pair. We exclude the pairs that contain *f*-valence electrons since DFT is hard to describe the strong correlation effect of these very localized electronic states.[44] After that, out of 3310 structures, 3234 converged ones are obtained. The convex hull analysis is then used to evaluate their thermodynamical stabilities. By utilizing the data from Materials Project,[31] the phase diagrams at 0 K are built and those with $E_{hull} \leq 0.1$ eV/atom are considered as thermodynamically stable (see Figure S6), which remains 900 structures. It is found that 100 of them can be found at Materials Project, which are no longer considered for further investigation. To reduce computational costs, we only explore the lattice-dynamical stabilities of 481 structures with cubic, tetragonal, orthorhombic, and hexagonal/trigonal symmetries and reasonable stacking orderings (details can be found in Figure S7) are calculated. At last, 353 of them are found to be lattice-dynamically stable without any imaginary frequencies or only small ones in the whole phonon spectra. Their phonon spectra are listed at the Supporting Information.

By a statistic of the number of elements in the unit cell, we find that most of them are ternary and quaternary structures

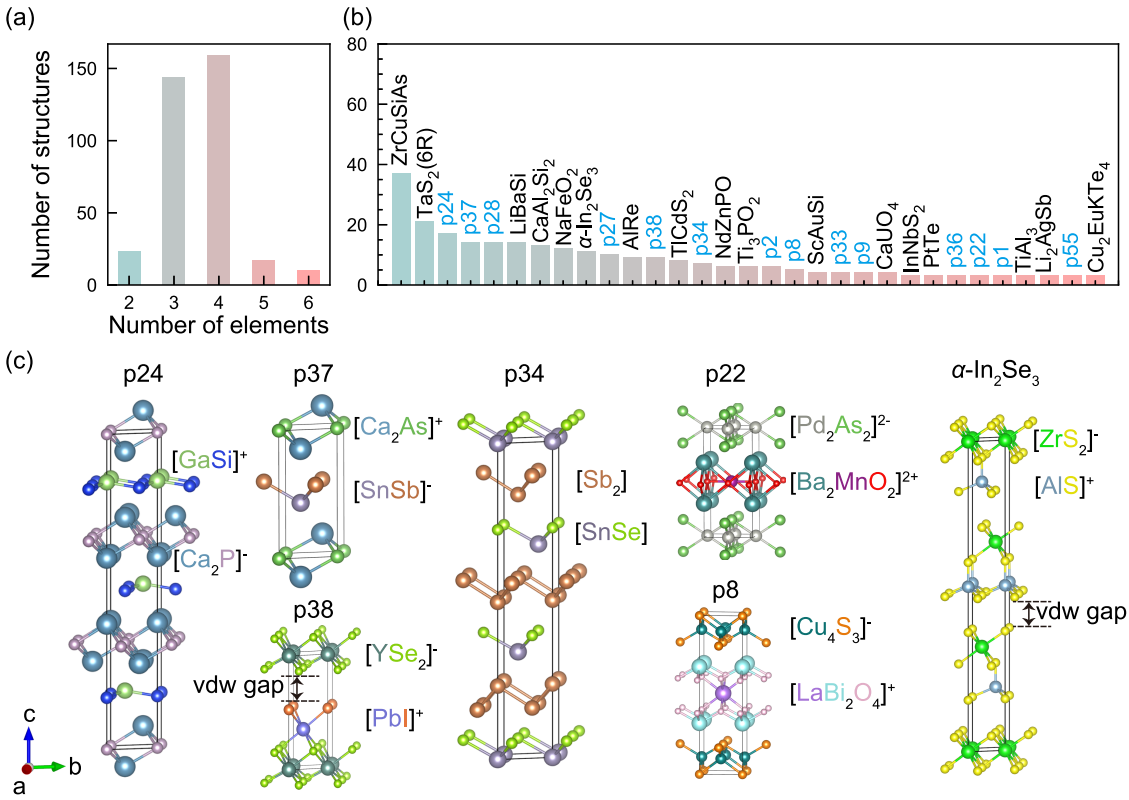

Figure 3. Statistics of the newly discovered 353 structures. (a) Element number distribution for the newly designed structures. (b) Classification of structures according to their prototypes. The black ones are defined in ICSD, and the blue ones are newly discovered ones. Note that the prototypes with number of structures less than 3 are not shown here. (c) Crystal structure of prototypes (partly).

https://doi.org/10.1021/acs.nanolett.3c01237
Nano Lett. 2023, 23, 4634−4641

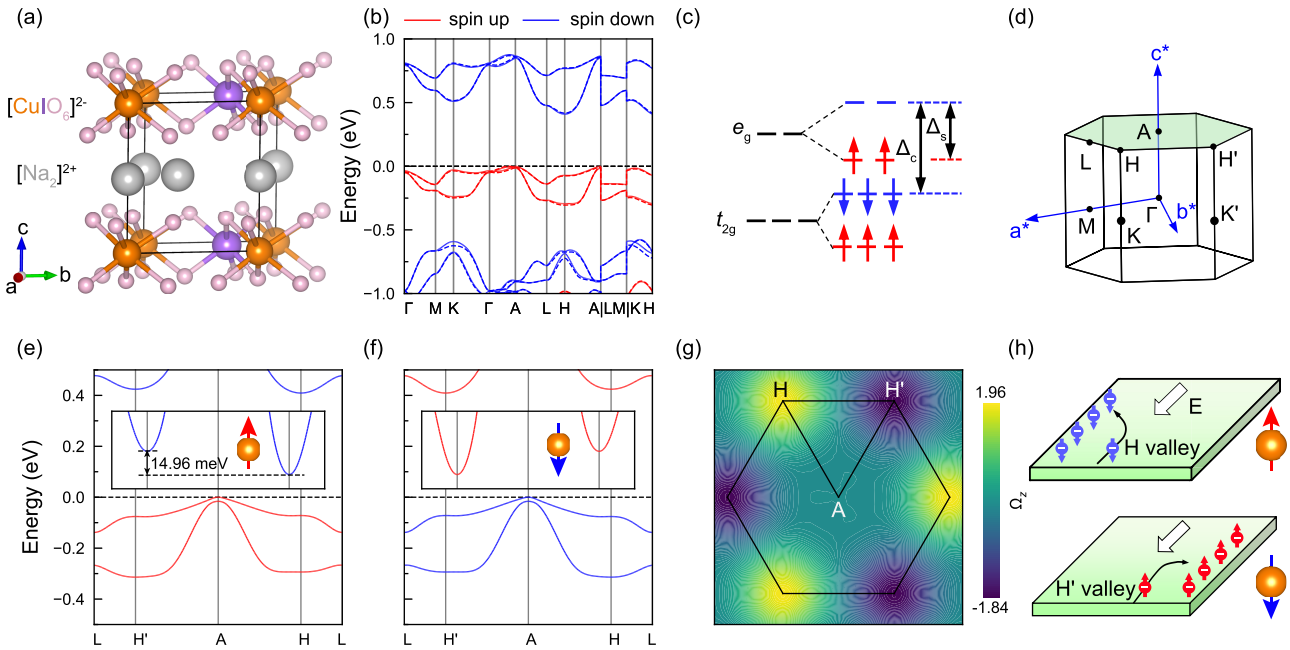

Figure 4. Bipolar ferromagnetic semiconducting and anomalous valley Hall effect of Na_2CuIO_6. (a) Crystal structure, (b) electronic structure without SOC (dashed line) and with SOC (solid line), (c) electron occupations of Cu 3d orbitals, (d) Brillouin zone (BZ), valley-splitting with Cu spins aligning (e) $+z$ direction and (f) $-z$ direction, (g) Berry curvature at k = 0.5 plane (Cu spins aligning $+z$ direction), and (h) schematic diagram of anomalous valley Hall effect for Na_2CuIO_6. The green surface in BZ shows k_z = 0.5 plane.

shown in Figure 3a. We then classify these new structures into different structural prototypes according to their space groups, Wyckoff positions, Pearson symbols, and structural similarity.[45,46] They are grouped into 99 prototypes in Figure 3b, and more than half of them are not defined in ICSD.[46] The most common structural prototype is ZrCuSiAs, which contains 37 similar structures in the subset. Although some of them share the same building-block prototypes, the stacking orderings or rotational/mirror operations can give rise to different structures. Such cases occur in p24, p37, p38 prototypes in Figures 3c, where all of them consist of $[CdI_2]$ and $[\alpha\text{-GeTe}]$ type building blocks but show distinct structures. Moreover, the atoms in building blocks can "rebond" to form new layers in part of structures as in p34, where the original building blocks are $[SnSb]^-$ and $[SbSe]^+$. Nevertheless, most of them are alternatively stacking of negative and positive charged building blocks.

It is found that 26 structures can be considered as vdW layered materials, such as α-In_2Se_3 prototype and p38 in Figure 3c, where covalent bonds form between two building blocks and become one layer. Further calculations inclusion of DFT-D3[47,48] corrections show reduced interlayer distance, confirming the vdW gap in between.

■ DISCOVERY OF FUNCTIONAL MATERIALS

We turn to investigate their electronic structures in order to find functional materials. Their electronic structures are calculated under the PBE functional level and can be found in Supporting Information. We find that more than half of them (184) are nonmagnetic (NM) metals, and the others are 124 NM semiconductors, 21 magnetic semiconductors, and 24 magnetic metals. Given the abundant electronic structures of these layered materials, we discuss their functionalities, some of which are elaborated below.

Among the 21 magnetic semiconductors, we further identify their ground states by comparing the total energies of different magnetic orderings including ferromagnetic and several antiferromagnetic orderings (details can be found in Figure S8). Only one of them shows ferromagnetic ground state, while the others are antiferromagnets. Figure 4a and Figure S9 show the crystal structure of the ferromagnetic semiconductor Na_2CuIO_6 with space group $P312$. It consists of $[CuIO_6]^{2-}$ charged layers with two Na^+ ions intercalating between them. The electronic structure both with and without spin−orbit coupling (SOC) in Figure 4b shows a typical bipolar magnetic semiconducting behavior with opposite spin for valence band (VB) and conduction band (CB). With applying a gate voltage, the Fermi level can be effectively tuned so that the spin orientations of electrons at Fermi level can be switched between spin up and spin down, which can be used as spin filter, spin valve, or spin separators.[49] This bipolar magnetic semiconducting behavior can be understood from the crystal field theory point of view. Figure 4c shows the energy level evolution and electron occupation of Cu in Na_2CuIO_6. The nominal valence state for Na, I, O, and Cu is +1, + 7, −2, and +3 so that Cu has $[Ar]3d^8$ electron configuration. Under the octahedral crystal field (Figure S9c), the d orbitals split into t_{2g} ($d_{xy}/d_{xz}/d_{yz}$) and e_g ($d_{x^2-y^2}/d_{z^2}$) groups, and t_{2g} orbitals are fully occupied and two electrons leave in the spin up channel of e_g orbitals, resulting in a magnetic moment 2 μ_B. Moreover, the crystal-field-induced gap Δ_c is larger than the exchange splitting Δ_s.[50,51] Thus, the bandgap lies between e_g of spin-up channel (CB) and spin-down channel (VB), leading to the bipolar magnetic semiconducting band structure.

Beyond that, the lack of centrosymmetry in conjunction with ferromagnetism in Na_2CuIO_6 gives rise to spontaneously polarized valleys, i.e., ferrovalley,[52] which can be used in processing information with valley degree of freedom. Compared with degenerate energy at conduction band minima (CBM) H and H' without considering SOC, the electronic

https://doi.org/10.1021/acs.nanolett.3c01237
Nano Lett. 2023, 23, 4634−4641

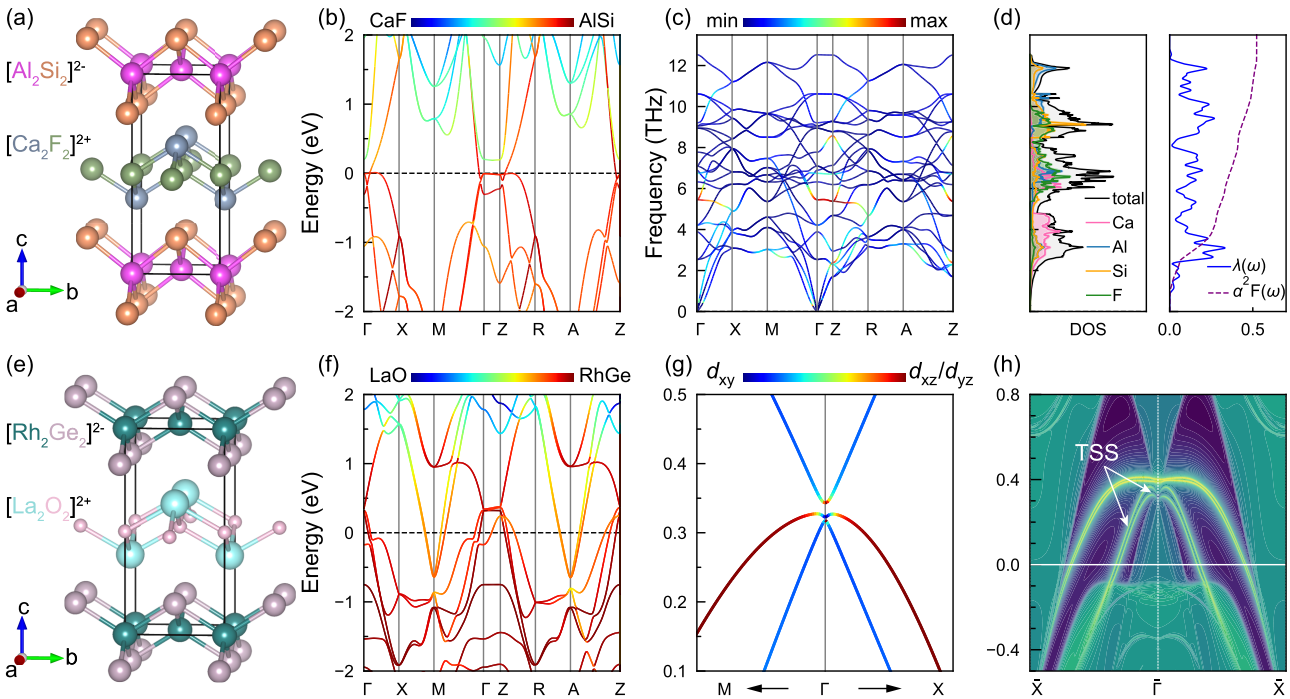

Figure 5. Superconductivity of CaAlSiF and band topology of LaRhGeO. (a) Crystal structure, (b) electronic structure, (c) phonon dispersion, (d) phonon density of states (left) and Eliashberg function $\alpha^2F(\omega)$ as well as the electron−phonon coupling strength $\lambda(\omega)$ (right) for CaAlSiF. (e) Crystal structure, (f) electronic structure, and (g) orbital-resolved band structure around Γ point with spin−orbit coupling, and (h) topological surface state (TSS) of (010) plane for LaRhGeO. The color in the electronic structure indicates the states contributed by distinct elements/orbitals, and that in the phonon dispersion shows the strength of electron−phonon coupling $\lambda_{q\nu}$.

structure with SOC shows a valley polarization of 14.96 meV (Figure 4e) with spins of Cu aligning +z axis. In contrast, when the magnetization direction aligns −z axis, the CBM changes from H to H′ alongside with spin reversal (Figure 4f). Accompanied by the valley polarization, the Berry curvature Ω_z of k_z = 0.5 plane (green region in Figure 4d) in Figure 4g shows opposite signs but unequal magnitudes of H (1.96) and H′ (−1.84) points, which renders an equivalent magnetic field for intriguing anomalous valley Hall effect (AVHE). When the system is electron doped for magnetization along +z direction, the spin-down electron at H valley will acquire an anomalous velocity v under the in-plane electric field E, i.e., $v \sim E \times \Omega(k)$, and move to the left side of the sample shown in the upper panel in Figure 4h. On the contrary, by reversing the magnetization direction, the spin-up electron at H′ valley will move to the right side of the sample shown in the lower panel in Figure 4h. Therefore, the Hall voltage can be readily detected with the accumulation of electron at one side, facilitating the observation of AVHE. We emphasize that the bipolar magnetic semiconductivity and AVHE are absent in its parent compound $KCuIO_6$ (Material Project ID mp-1147553) which is a half metal in its electronic structure. These emergent phenomena are induced by the change of charge state in $[CuIO_6]^{\delta-}$ functional building block. Moreover, Cu^{3+} and $[IO_6]^{5-}$ exist in real materials, e.g., $KCuO_2$ [53] and $Sr_5(IO_6)_2$,[54] which is beneficial for experimentally for experimentally synthesizing Na_2CuIO_6.

Next, we discover superconducting materials among them. We notice that $[Al_2Si_2]^{2-}$ embeds with superconductivity; for that the parent compound NaAlSi is a superconductor with transition temperature $T_c \approx 7$ K.[55,56] Here, a structure CaAlSiF crystallized with ZrCuSiAs structural prototype is shown in Figure 5a. Moreover, we find that the electronic structure in Figure 5b is similar to that of NaAlSi,[57] and the states of Al and Si dominate the Fermi level. Figure 5c shows its phonon dispersion together with electron−phonon coupling (EPC) strength $\lambda_{q\nu}$ for mode ν at wavevector q point. It shows that modes around 9 THz at Z point and modes between 4.5 and 6 THz contribute most to the EPC. We further calculate Eliashberg function $\alpha^2F(\omega)$ and EPC strength $\lambda(\omega)$ in Figure 5d. Utilizing McMillan formula,[58] we obtained T_c = 3 K with λ = 0.53 and effective screened Coulomb repulsion constant of μ^* = 0.1, confirming its superconductivity. As a comparison, our calculated EPC strength λ and T_c for NaAlSi are 0.4 and 1.01 K (Figure S10), respectively, indicating that CaFAlSi possibly has a higher superconducting transition temperature than NaAlSi once it is synthesized. Similarly, we predict that Ba_2F_2PtAs is also a superconductor with T_c = 1.5 K (see Figure S11), which is close to $T_c \approx 2.4$ K [59,60] in SrPtAs.

Finally, we find topological materials among them. We notice that building blocks with PbO-type structure possibly harbor nontrivial band topology.[61,62] Our predicted LaRhGeO, crystallized with ZrCuSiAs structure shown in Figure 5e, is a good candidate in this respect. The electronic structure in Figure 5f is similar to that of CoX (X = As, Sb, Bi).[61,62] At Γ point above the Fermi level 0.33 eV, the bands are mainly composed of Rh-d_{xy}, d_{yz}, and d_{xz} orbitals. By considering SOC, it displays a band inversion around Γ point (see Figure 5g), driving the system into a topological nontrivial phase. The Wannier charge center evolution of LaRhGeO in Figure S12 gives rise to $\mathbb{Z}_2$ = (0;001), indicating the nontrivial band topology. Then the local density of states (LDOS) for (010) surface is calculated, shown in Figure 5h, which exhibits topologically protected surface states, further confirming the nontrivial band topology.

https://doi.org/10.1021/acs.nanolett.3c01237
Nano Lett. 2023, 23, 4634−4641

Except for these functional materials, the chemical and physical properties of other materials are largely unexplored. For example, α-In_2Se_3 prototype of the predicted magnetic material $AlCrS_3$ possibly endows itself with ferroelectric property, making it a candidate for multiferroic materials, which deserve further investigation.

DISCUSSION

We discuss several aspects in designing layered materials. First, multilayer functional layered materials can be tried by utilizing the database because we only stack two charged building blocks and the new structures we designed here contain only one functional building block. Second, this layer-by-layer stacking method is beneficial for designing multiple elemental materials, e.g., ternary, quaternary, and quinary compounds, because the Born−Oppenheimer energy surface of them is complicated. Stacking these building blocks is possibly a fast way to find potential stable/metastable layered materials with multiple elements, and we indeed find plenty of materials with more than four elements (Figure 3a). Third, this design method by stacking of building blocks not only is applicable for 2D building blocks but also can be extended to 1D and 0D building blocks. Besides, heterodimensional building blocks can also be tried to make a crystal, e.g., 2D + 1D building blocks.[63,64]

In conclusion, we have demonstrated an effective workflow to design functional materials by stacking of two-dimensional charged building blocks with commensurate lattice and charge balance. This method is conducted based on our constructed two-dimensional building block database. It contains 1208 building blocks which display versatility in terms of prototypes, crystal systems, elemental distributions, and functionalities. We discover 353 energetically favorable and lattice-dynamically stable structures by stacking of these building blocks with the help of density functional calculations. Moreover, we find superconductors $CaAlSiF/Ba_2F_2PtAs$, a bipolar ferromagnetic semiconductor Na_2CuIO_6 with valley polarization, and a topological material LaRhGeO among them. Other functional materials with inherited/enhanced/emergent performance are still waiting to be exploited. This layer-by-layer stacking strategy also provides an alternative route for exploring multifunctional, multielemental, and heterodimensional materials.

ASSOCIATED CONTENT

Supporting Information

The Supporting Information is available free of charge at https://pubs.acs.org/doi/10.1021/acs.nanolett.3c01237.

Details for the database construction; details for building layered structures; statistics of calculated E_{hull} values; example of structure with unreasonable stacking ordering; high-through calculation of the ground state for magnetic materials; additional views for Na_2CuIO_6; superconductivity of Ba_2F_2PtAs and NaAlSi; calculation details; full list of predicted 353 stable structures and their band structures/phonon spectra; table of 1208 charged building blocks found in this work (PDF)

2D charged building block database (PDF)

AUTHOR INFORMATION

Corresponding Author

Shixuan Du − *Beijing National Laboratory for Condensed Matter Physics, Institute of Physics, Chinese Academy of Sciences, Beijing 100190, China; School of Physics, University of Chinese Academy of Sciences, Beijing 100049, China; Songshan Lake Materials Laboratory, Dongguan, Guangdong 523808, China;* orcid.org/0000-0001-9323-1307; Email: sxdu@iphy.ac.cn

Authors

Jun Deng − *Beijing National Laboratory for Condensed Matter Physics, Institute of Physics, Chinese Academy of Sciences, Beijing 100190, China;* orcid.org/0000-0003-2420-8079

Jinbo Pan − *Beijing National Laboratory for Condensed Matter Physics, Institute of Physics, Chinese Academy of Sciences, Beijing 100190, China; School of Physics, University of Chinese Academy of Sciences, Beijing 100049, China; Songshan Lake Materials Laboratory, Dongguan, Guangdong 523808, China*

Yan-Fang Zhang − *School of Physics, University of Chinese Academy of Sciences, Beijing 100049, China*

Complete contact information is available at: https://pubs.acs.org/10.1021/acs.nanolett.3c01237

Author Contributions

S.D. and J.D. directed the project. J.D. performed database construction, structure design, and density functional calculations. All authors analyzed the data and wrote, revised, and gave approval to the final version of the manuscript.

Notes

The authors declare no competing financial interest.

ACKNOWLEDGMENTS

We thank X. L. Chen, J. T. Sun, W. H. Dong for their helpful discussions. This work was supported by grants from the National Natural Science Foundation of China (Grants 61888102, 52272172, and 52102193), the Major Program of National Natural Science Foundation of China (Grant 92163206), the National Key Research and Development Program of China (Grant 2021YFA1201501), Key R&D of the Ministry of Science and Technology (Grant 2022YFA-1204100), the Strategic Priority Research Program of the Chinese Academy of Sciences (XDB30000000), and the Fundamental Research Funds for the Central Universities. Computational resources were provided by the National Supercomputing Center in Tianjin.

REFERENCES

(1) McKinney, R. W.; Gorai, P.; Manna, S.; Toberer, E.; Stevanović, V. Ionic vs. van der Waals layered materials: identification and comparison of elastic anisotropy. *J. Mater. Chem. A* **2018**, *6* (32), 15828−15838.

(2) Gong, C.; Zhang, X. Two-dimensional magnetic crystals and emergent heterostructure devices. *Science* **2019**, *363* (6428), eaav4450.

(3) Pan, J.; Yu, J.; Zhang, Y.-F.; Du, S.; Janotti, A.; Liu, C.-X.; Yan, Q. Quantum anomalous Hall effect in two-dimensional magnetic insulator heterojunctions. *npj Comput. Mater.* **2020**, *6*, 152.

(4) Novoselov, K. S.; Mishchenko, A.; Carvalho, A.; Castro Neto, A. H. 2D materials and van der Waals heterostructures. *Science* **2016**, *353* (6298), aac9439.

(5) Geim, A. K.; Grigorieva, I. V. Van der Waals heterostructures. *Nature* **2013**, *499* (7459), 419−425.
(6) Gong, C.; Kim, E. M.; Wang, Y.; Lee, G.; Zhang, X. Multiferroicity in atomic van der Waals heterostructures. *Nat. Commun.* **2019**, *10* (1), 2657.
(7) Kabbour, H.; Cario, L.; Boucher, F. Rational design of new inorganic compounds with the ZrSiCuAs structure type using 2D building blocks. *J. Mater. Chem. A* **2005**, *15* (34), 3525−3531.
(8) Cario, L.; Kabbour, H.; Meerschaut, A. Designing new inorganic compounds from 2D building blocks. *Chem. Mater.* **2005**, *17* (2), 234−236.
(9) Kabbour, H.; Cario, L. $Ae_2Sb_2X_4F_2$ (Ae = Sr, Ba): New Members of the Homologous Series $Ae_2M_{1+n}X_{3+n}F_2$ Designed from Rock Salt and Fluorite 2D Building Blocks. *Inorg. Chem.* **2006**, *45* (6), 2713.
(10) Kabbour, H.; Cario, L.; Danot, M.; Meerschaut, A. Design of a New Family of Inorganic Compounds $Ae_2F_2SnX_3$ (Ae = Sr, Ba; X = S, Se) Using Rock Salt and Fluorite 2D Building Blocks. *Inorg. Chem.* **2006**, *45* (2), 917.
(11) Sun, Y. L.; Ablimit, A.; Zhai, H. F.; Bao, J. K.; Tang, Z. T.; Wang, X. B.; Wang, N. L.; Feng, C. M.; Cao, G. H. Design and synthesis of a new layered thermoelectric material $LaPbBiS_3O$. *Inorg. Chem.* **2014**, *53* (20), 11125−9.
(12) Kamihara, Y.; Watanabe, T.; Hirano, M.; Hosono, H. Iron-Based Layered Superconductor $La[O_{1-x}F_x]FeAs$ (x=0.05-0.12) with T_c = 26 K. *J. Am. Chem. Soc.* **2008**, *130* (11), 3296−3297.
(13) Yang, J.; Li, Z.-C.; Lu, W.; Yi, W.; Shen, X.-L.; Ren, Z.-A.; Che, G.-C.; Dong, X.-L.; Sun, L.-L.; Zhou, F.; Zhao, Z.-X. Superconductivity at 53.5 K in $GdFeAsO_{1-\delta}$. *Supercond. Sci. Technol.* **2008**, *21* (8), 082001.
(14) Chen, G. F.; Li, Z.; Wu, D.; Li, G.; Hu, W. Z.; Dong, J.; Zheng, P.; Luo, J. L.; Wang, N. L. Superconductivity at 41 K and its competition with spin-density-wave instability in layered $CeO_{1-x}F_xFeAs$. *Phys. Rev. Lett.* **2008**, *100* (24), 247002.
(15) Ju, J.; Li, Z.; Mu, G.; Wen, H. H.; Sato, K.; Watahiki, M.; Li, G.; Tanigaki, K. A structural study of the hole-doped superconductors $Pr_{1-x}Sr_xFeAsO$. *New J. Phys.* **2009**, *11* (8), 083003.
(16) Wen, H.-H.; Mu, G.; Fang, L.; Yang, H.; Zhu, X. Superconductivity at 25 K in hole-doped $(La_{1-x}Sr_x)OFeAs$. *EPL* **2008**, *82* (1), 17009.
(17) Yuri, I.; Ernst, K. *High-T_c Superconductors Based on FeAs Compounds*. Springer Berlin: Heidelberg, Germany, 2010; pp 5−6.
(18) Gibson, Q. D.; Dyer, M. S.; Whitehead, G. F. S.; Alaria, J.; Pitcher, M. J.; Edwards, H. J.; Claridge, J. B.; Zanella, M.; Dawson, K.; Manning, T. D.; Dhanak, V. R.; Rosseinsky, M. J. $Bi_4O_4Cu_{1.7}Se_{2.7}Cl_{0.3}$: Intergrowth of BiOCuSe and Bi_2O_2Se Stabilized by the Addition of a Third Anion. *J. Am. Chem. Soc.* **2017**, *139* (44), 15568−15571.
(19) Gibson, Q. D.; Manning, T. D.; Zanella, M.; Zhao, T.; Murgatroyd, P. A. E.; Robertson, C. M.; Jones, L. A. H.; McBride, F.; Raval, R.; Cora, F.; Slater, B.; Claridge, J. B.; Dhanak, V. R.; Dyer, M. S.; Alaria, J.; Rosseinsky, M. J. Modular Design via Multiple Anion Chemistry of the High Mobility van der Waals Semiconductor $Bi_4O_4SeCl_2$. *J. Am. Chem. Soc.* **2020**, *142* (2), 847−856.
(20) Liang, Y.; Zhou, X.; Li, W.; Peng, H. Preparation of two-dimensional $[Bi_2O_2]$-based layered materials: Progress and prospects. *APL Mater.* **2021**, *9* (6), 060905.
(21) Singh, Y.; Green, M. A.; Huang, Q.; Kreyssig, A.; McQueeney, R. J.; Johnston, D. C.; Goldman, A. I. Magnetic order in $BaMn_2As_2$ from neutron diffraction measurements. *Phys. Rev. B* **2009**, *80* (10), No. 100403(R).
(22) Emery, N.; Wildman, E. J.; Skakle, J. M.; Giriat, G.; Smith, R. I.; McLaughlin, A. C. Giant magnetoresistance in oxypnictides (La,Nd)-OMnAs. *Chem. Commun.* **2010**, *46* (36), 6777.
(23) Wildman, E. J.; Skakle, J. M.; Emery, N.; McLaughlin, A. C. Colossal magnetoresistance in Mn^{2+} oxypnictides $NdMnAsO_{1-x}F_x$. *J. Am. Chem. Soc.* **2012**, *134* (21), 8766.
(24) McGuire, M. A.; Garlea, V. O. Short- and long-range magnetic order in LaMnAsO. *Phys. Rev. B* **2016**, *93* (5), 054404.
(25) Atikur Rahman, M. A Review on Cuprate Based Superconducting Materials Including Characteristics and Applications. *Am. J. Phys. Appl.* **2015**, *3* (2), 39−56.
(26) Kordyuk, A. A. Iron-based superconductors: Magnetism, superconductivity, and electronic structure (Review Article). *Low Temp. Phys.* **2012**, *38* (9), 888−899.
(27) Zhou, Q.; Lu, S.; Wu, Y.; Wang, J. Property-Oriented Material Design Based on a Data-Driven Machine Learning Technique. *J. Phys. Chem. Lett.* **2020**, *11* (10), 3920−3927.
(28) Chen, L.; Zhang, X.; Chen, A.; Yao, S.; Hu, X.; Zhou, Z. Targeted design of advanced electrocatalysts by machine learning. *Chin. J. Catal.* **2022**, *43* (1), 11−32.
(29) Chen, A.; Zhang, X.; Zhou, Z. Machine learning: Accelerating materials development for energy storage and conversion. *InfoMat* **2020**, *2* (3), 553−576.
(30) Ashton, M.; Paul, J.; Sinnott, S. B.; Hennig, R. G. Topology-Scaling Identification of Layered Solids and Stable Exfoliated 2D Materials. *Phys. Rev. Lett.* **2017**, *118* (10), 106101.
(31) Jain, A.; Ong, S. P.; Hautier, G.; Chen, W.; Richards, W. D.; Dacek, S.; Cholia, S.; Gunter, D.; Skinner, D.; Ceder, G.; Persson, K. A. Commentary: The Materials Project: A materials genome approach to accelerating materials innovation. *APL Mater.* **2013**, *1* (1), 011002.
(32) Barber, C. B.; Dobkin, D. P.; Huhdanpaa, H. The Quickhull Algorithm for Convex Hulls. *ACM Trans. Math. Softw.* **1996**, *22* (4), 469−483.
(33) Ong, S. P.; Wang, L.; Kang, B.; Ceder, G. Li−Fe−P−O_2 Phase Diagram from First Principles Calculations. *Chem. Mater.* **2008**, *20* (5), 1798−1807.
(34) Ong, S. P.; Richards, W. D.; Jain, A.; Hautier, G.; Kocher, M.; Cholia, S.; Gunter, D.; Chevrier, V. L.; Persson, K. A.; Ceder, G. Python Materials Genomics (pymatgen): A robust, open-source python library for materials analysis. *Comput. Mater. Sci.* **2013**, *68*, 314−319.
(35) Sato, T.; Nakayama, K.; Sekiba, Y.; Richard, P.; Xu, Y. M.; Souma, S.; Takahashi, T.; Chen, G. F.; Luo, J. L.; Wang, N. L.; Ding, H. Band structure and fermi surface of an extremely overdoped iron-based superconductor KFe_2As_2. *Phys. Rev. Lett.* **2009**, *103* (4), 047002.
(36) Rotter, M.; Pangerl, M.; Tegel, M.; Johrendt, D. Superconductivity and Crystal Structures of $(Ba_{1-x}K_x)Fe_2As_2$(x = 0−1). *Angew. Chem., Int. Ed.* **2008**, *47* (41), 7949−7952.
(37) Kamihara, Y.; Hiramatsu, H.; Hirano, M.; Kawamura, R.; Yanagi, H.; Kamiya, T.; Hosono, H. Iron-based layered superconductor: LaOFeP. *J. Am. Chem. Soc.* **2006**, *128* (31), 10012−10013.
(38) Guo, J.; Jin, S.; Wang, G.; Wang, S.; Zhu, K.; Zhou, T.; He, M.; Chen, X. Superconductivity in the iron selenide $K_xFe_2Se_2(0 \leq x \leq 1.0)$. *Phys. Rev. B* **2010**, *82* (18), 180520.
(39) Zheng, H.; Li, X.-B.; Chen, N.-K.; Xie, S.-Y.; Tian, W. Q.; Chen, Y.; Xia, H.; Zhang, S. B.; Sun, H.-B. Monolayer II-VI semiconductors: A first-principles prediction. *Phys. Rev. B* **2015**, *92* (11), 115307.
(40) Attia, A. A.; Jappor, H. R. Tunable electronic and optical properties of new two-dimensional GaN/BAs van der Waals heterostructures with the potential for photovoltaic applications. *Chem. Phys. Lett.* **2019**, *728*, 124−131.
(41) Lepley, N. D.; Holzwarth, N. A. W. Modeling interfaces between solids: Application to Li battery materials. *Phys. Rev. B* **2015**, *92* (21), 214201.
(42) Wolloch, M.; Losi, G.; Chehaimi, O.; Yalcin, F.; Ferrario, M.; Righi, M. C. High-throughput generation of potential energy surfaces for solid interfaces. *Comput. Mater. Sci.* **2022**, *207*, 111302.
(43) Perdew, J. P.; Burke, K.; Ernzerhof, M. Generalized gradient approximation made simple. *Phys. Rev. Lett.* **1996**, *77* (18), 3865−3868.
(44) Kirklin, S.; Saal, J. E.; Meredig, B.; Thompson, A.; Doak, J. W.; Aykol, M.; Rühl, S.; Wolverton, C. The Open Quantum Materials Database (OQMD): assessing the accuracy of DFT formation energies. *npj Comput. Mater.* **2015**, *1* (1), 15010.

https://doi.org/10.1021/acs.nanolett.3c01237
Nano Lett. 2023, 23, 4634−4641

(45) Hicks, D.; Toher, C.; Ford, D. C.; Rose, F.; Santo, C. D.; Levy, O.; Mehl, M. J.; Curtarolo, S. AFLOW-XtalFinder: a reliable choice to identify crystalline prototype. *npj Comput. Mater.* **2021**, *7* (1), 30.
(46) Allmann, R.; Hinek, R. The introduction of structure types into the Inorganic Crystal Structure Database ICSD. *Acta Crystallogr., Sect. A* **2007**, *63* (5), 412−417.
(47) Grimme, S.; Ehrlich, S.; Goerigk, L. Effect of the Damping Function in Dispersion Corrected Density Functional Theory. *J. Comput. Chem.* **2011**, *32* (7), 1456−1465.
(48) Grimme, S.; Antony, J.; Ehrlich, S.; Krieg, H. A consistent and accurate ab initio parametrization of density functional dispersion correction (DFT-D) for the 94 elements H-Pu. *J. Chem. Phys.* **2010**, *132* (15), 154104.
(49) Li, X.; Wu, X.; Li, Z.; Yang, J.; Hou, J. G. Bipolar magnetic semiconductors: a new class of spintronics materials. *Nanoscale* **2012**, *4* (18), 5680−5685.
(50) Deng, J.; Pan, J.; Zhang, Y.; Li, Y.; Dong, W.; Sun, J.; Du, S. Screening and Design of Bipolar Magnetic-Semiconducting Monolayers and Heterostructures. *ACS Appl. Electron. Mater.* **2022**, *4* (7), 3232−3239.
(51) Deng, J.; Guo, J.; Hosono, H.; Ying, T.; Chen, X. Two-dimensional bipolar ferromagnetic semiconductors from layered antiferromagnets. *Phys. Rev. Mater.* **2021**, *5* (3), 034005.
(52) Tong, W.-Y.; Gong, S.-J.; Wan, X.; Duan, C.-G. Concepts of ferrovalley material and anomalous valley Hall effect. *Nat. Commun.* **2016**, *7* (1), 13612.
(53) Choudhury, D.; Rivero, P.; Meyers, D.; Liu, X.; Cao, Y.; Middey, S.; Whitaker, M. J.; Barraza-Lopez, S.; Freeland, J. W.; Greenblatt, M.; Chakhalian, J. Anomalous charge and negative-charge-transfer insulating state in cuprate chain compound $KCuO_2$. *Phys. Rev. B* **2015**, *92* (20), 201108.
(54) Hummel, T.; Salk, F.; Ströbele, M.; Enseling, D.; Jüstel, T.; Meyer, H. J. The Orthoperiodates of Calcium, Strontium, and Barium. *Eur. J. Inorg. Chem.* **2015**, *2015* (6), 977−981.
(55) Kuroiwa, S.; Kawashima, H.; Kinoshita, H.; Okabe, H.; Akimitsu, J. Superconductivity in ternary silicide NaAlSi with layered diamond-like structure. *Phys. C: Supercond. Appl.* **2007**, *466* (1−2), 11−15.
(56) Yamada, T.; Hirai, D.; Yamane, H.; Hiroi, Z. Superconductivity in the Topological Nodal-line Semimetal NaAlSi. *J. Phys. Soc. Jpn.* **2021**, *90* (3), 034710.
(57) Jin, L.; Zhang, X.; He, T.; Meng, W.; Dai, X.; Liu, G. Topological nodal line state in superconducting NaAlSi compound. *J. Mater. Chem. C* **2019**, *7* (34), 10694−10699.
(58) McMillan, W. L. Transition Temperature of Strong-Coupled Superconductors. *Phys. Rev.* **1968**, *167* (2), 331−344.
(59) Youn, S. J.; Fischer, M. H.; Rhim, S. H.; Sigrist, M.; Agterberg, D. F. Role of strong spin-orbit coupling in the superconductivity of the hexagonal pnictide SrPtAs. *Phys. Rev. B* **2012**, *85* (22), 220505.
(60) Nishikubo, Y.; Kudo, K.; Nohara, M. Superconductivity in the Honeycomb-Lattice Pnictide SrPtAs. *J. Phys. Soc. Jpn.* **2011**, *80* (5), 055002.
(61) Gao, J.; Ding, W.; Zhang, S.; Zhang, Z.; Cui, P. Coexistence of Superconductivity and Nontrivial Band Topology in Monolayered Cobalt Pnictides on $SrTiO_3$. *Nano Lett.* **2021**, *21* (17), 7396−7404.
(62) Ding, W.; Zeng, J.; Qin, W.; Cui, P.; Zhang, Z. Exploring High Transition Temperature Superconductivity in a Freestanding or $SrTiO_3$-Supported CoSb Monolayer. *Phys. Rev. Lett.* **2020**, *124* (2), 027002.
(63) Zhou, J.; Zhang, W.; Lin, Y.-C.; Cao, J.; Zhou, Y.; Jiang, W.; Du, H.; Tang, B.; Shi, J.; Jiang, B.; Cao, X.; Lin, B.; Fu, Q.; Zhu, C.; Guo, W.; Huang, Y.; Yao, Y.; Parkin, S. S. P.; Zhou, J.; Gao, Y.; Wang, Y.; Hou, Y.; Yao, Y.; Suenaga, K.; Wu, X.; Liu, Z. Heterodimensional superlattice with in-plane anomalous Hall effect. *Nature* **2022**, *609* (7925), 46−51.
(64) Cheon, G.; Duerloo, K. N.; Sendek, A. D.; Porter, C.; Chen, Y.; Reed, E. J. Data Mining for New Two- and One-Dimensional Weakly Bonded Solids and Lattice-Commensurate Heterostructures. *Nano Lett.* **2017**, *17* (3), 1915−1923.

Recommended by ACS

Dominant Two-Dimensional Electron–Phonon Interactions in the Bulk Dirac Semimetal Na_3Bi

Dhruv C. Desai, Marco Bernardi, *et al.*
APRIL 24, 2023
NANO LETTERS
READ

Theoretical Prediction of Antiferromagnetic Skyrmion Crystal in Janus Monolayer $CrSi_2N_2As_2$

Kaiying Dou, Yandong Ma, *et al.*
NOVEMBER 30, 2022
ACS NANO
READ

Gate and Temperature Driven Phase Transitions in Few-Layer $MoTe_2$

Hugo Kowalczyk, Abhay Shukla, *et al.*
MARCH 27, 2023
ACS NANO
READ

First-Principles Study of Structural and Electronic Properties of Monolayer PtX_2 and Janus PtXY (X, Y = S, Se, and Te) via Strain Engineering

Xun Ge, Xiaoshuang Chen, *et al.*
FEBRUARY 03, 2023
ACS OMEGA
READ

Get More Suggestions >

https://doi.org/10.1021/acs.nanolett.3c01237
Nano Lett. 2023, 23, 4634−4641